Title
A simple method for improvement of mass resolution and isotope accuracy for laser ablation and ionisation time of flight mass spectrometers.

Authors
R. Wiesendanger, M. Tulej, V. Grimaudo, A. Cedeño López, R. Lukmanov, A. Riedo and P. Wurz

Abstract
Accumulation of spectra is a common approach for improvement of signal-to-noise ratio in mass spectrometry. However, severe degradation of the overall spectrum can occur if some individual mass spectra of bad quality are included in the accumulation process. In this contribution, we discuss potential sources of spectral distortions on the example of mass spectra measured by our miniature laser ablation/ionisation time-of-flight mass spectrometer and present a filtering method capable of systematic and reproducible identification and rejection of spectra of bad quality. Using this method, we were able to achieve a significant improvement of the signal-to-noise ratio and thus of isotope accuracy. By analysing the Si, Cr and Ni measurements acquired on a Trevorite mineral, we show that improvements of the isotope accuracy by factors between 1.6 and 7.7 can be achieved.

Key Words
Laser Ablation and Ionisation Time of Flight Mass Spectrometry (LIMS-TOF), Data Processing, Resolution, Sensitivity, Isotope Ratio, Accuracy

Introduction
Recent developments in Laser Ionisation Mass Spectrometer (LIMS) systems has led to significant improvements of quantitative performance in chemical analysis of solid materials [1-5]. Since their development time in the 1970'ties, LIMS instruments were used in the quantitative analysis of solid samples in combination with appropriate standard reference materials. In the early years of this century, the LIMS technique has been qualified as a semi-quantitative method. The quantitative performance is found to be primarily limited by the performance of the laser ion source[2, 4, 6] with its dependence on several laser parameters and the mass analyser with limited ion-optical transmission. With the progress in laser technology including developments of femtosecond laser sources, improvements of the mass analyser design and modelling tools, these fundamental limitations were substantially reduced during the last decade. The quantitative analysis of element and isotope abundances of various samples ranging from NIST standard materials to samples of rocks were recently demonstrated[7-8]. Nowadays the quantitative performance of a LIMS system has to be optimized depending on the instrument.

The miniature LIMS system considered in this contribution is a laser ablation/ionisation mass spectrometer coupled with a time-of-flight (TOF) mass analyser and was developed at the University of Bern. The instrument is named LMS (Laser Mass Spectrometer) and has been designed for the application in space research[9]. When placed on a planetary rover or a lander, the element and isotope analysis of planetary rocks and soils provides information on local mineralogy, and fractionation processes. These data can be used to determine times of formation of the planetary surface, provide insights into cosmochemical processes[3, 10-12], and even for detection of bio-signatures[10, 13-14].

In the current contribution, we consider LMS with its typical mass resolving power resulting from the combination of the spatial and energy distribution of the ions produced by a laser ion

source, the type of mass analyser and its size, and ion optical design parameters. The nominal performance may be reduced by two categories of effects degrading the recorded mass spectra.

The first category contains all random noise sources, which are minimised by the experimental setup with the remaining noise amplitude to be reduced by a purely statistical approach: Often hundreds to thousands of spectra are accumulated to enhance the signal-to-noise ratio (SNR) of a spectrum. This improves the measurement accuracy and the ability to detect trace elements. Using this accumulation process, one achieves an improvement in accuracy of the element abundance and isotope ratio, and a lowering of detection limits of trace elements[8, 15].

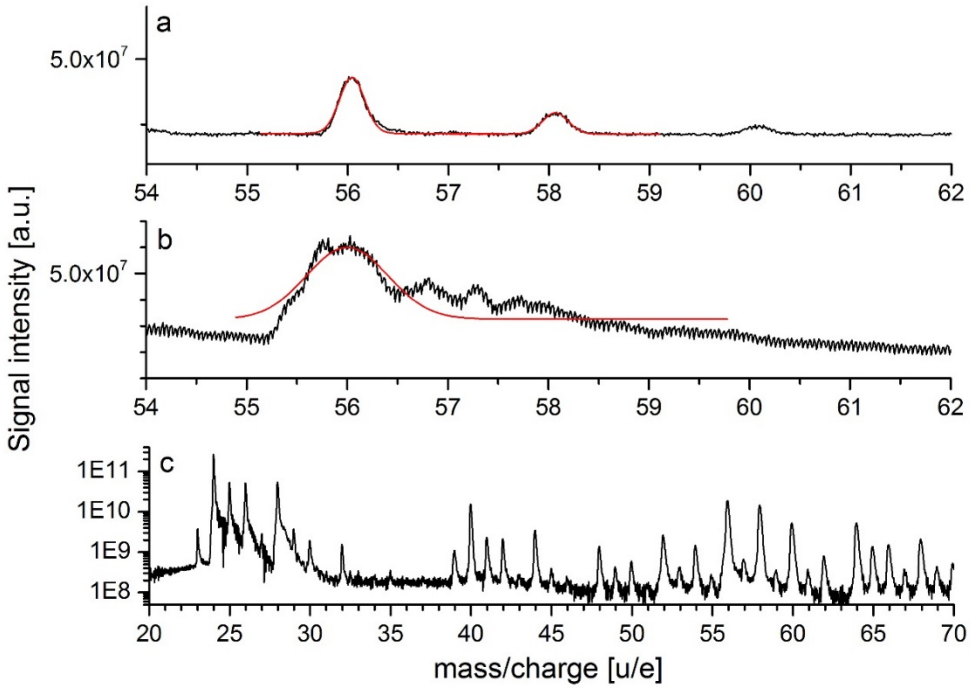

Figure 1: Detail of a mass spectrum of good quality before accumulation (panel a), distorted single spectrum before accumulation (panel b), and accumulation of 238 spectra (panel c) including the spectra in panel a and b.

The second category contains other distortion effects that cannot be mitigated by purely statistical means. One problem falling into this category is the limited shot to shot of the ablation laser, which is often a problem in laser ablation mass spectrometry. Especially when Q-switched lasers (e.g. Nd:YAG laser operating in the ns pulse range) are used the shot-to-shot fluctuations of the pulse energy can be as high as 40%. The Ti:Sapphire laser system used in our setup (operating with fs laser pulses) has a much better shot-to-shot pulse energy stability of less than 6 ‰[6] so that fluctuations of the laser power can be excluded as a reason for the observed degradations of the spectra.

The stability of the ion production is also limited by the surface quality of the sample. Large signal fluctuations are observed during the initial laser ablation shots, and also when studies are conducted on highly porous and heterogeneous samples. Moreover, high ion production rates can lead to distortion of the spectra either through charging of the sample surface or by space charge effects if the produced amount of ions charges causes noticeable columbic repulsion inside the ablated ion plume [12, 16]. In some extreme cases, the resulting spatial and energy spread of the ablated plume may then exceed the capabilities of energy and spatial focusing of the ion optical system, which results in mass spectra of low spectral resolution.

The second category also includes signal ringing due to impedance mismatch in the signal transmission line and capture of high frequency electromagnetic radiation that are introduced into the signal path through inductive or capacitive coupling (cross-talk).

Problems of the second category cannot be mitigated through accumulation of spectra and need to be tackled with dedicated measures. The isolation of these typically rare effects from the overall number of individual mass spectra is of considerable interest for improving the quantitative performance. In this contribution, we present a systematic method to remove degraded spectra from the accumulation process.

Figure 1 illustrates the effects of a few degraded mass spectra on the spectral quality of accumulation of 238 spectra. Panel *a* shows a well resolved single spectrum. If only spectra of this quality would be accumulated, the overall spectrum shown in panel c should contain only well-resolved mass peaks. However, the spectrum was obtained by the inclusion of several low resolution spectra, one example of these is it shown in panel b. These spectra have significantly lower mass resolution, show peak intensities fluctuating from shot to shot, and distorted mass peak shapes with an undefined baseline. After accumulation of all 238 spectra, the distorted spectra deteriorate the baseline (panel c). Large sections of the mass range between m/q = 20 and 32 or 52 and 63 are not usable for conducting precise isotope analysis. Also, identification of elements and their quantitative analysis would be very difficult.

A logic approach to improve the quantitative performance of the instrument is therefore to apply a suitable filtering method to exclude the few low-quality spectra before the accumulation process. This method should comply with a minimal set of requirements:

1. it must be repeatable
2. it should not bias the result by introducing a-priori knowledge.
3. for optimal usability, the process should also be highly automatized because a large amount of data needs to be processed.

Implementation

A simple method that complies with these requirements is to automatically analyse peak shape and attribute and evaluate a score (S) according to the spectral quality to each individual spectrum prior to the accumulation. The score is determined by comparing the measured mass peaks to an ideal peak profile. The profile contains two neighbouring mass peaks, which allows to assess the separation of the peaks. This is of particular interest when accurate isotope determination is required. In the simplest case, the two neighbouring peaks can be perfectly described by composing two Gaussian curves. Although this model is an over-simplification in many cases, it turned out to work sufficiently well in our case.

For the ideal peak profile, it is not sufficient to assume Gauss distributions with fixed parameters, because the intensity of the acquired signal can vary over a wide range during a measurement campaign, regardless of the quality of the spectrum. Using fixed parameters would therefore lead to a rejection of many spectra, for the sole reason of not being close to the profile parameters set by the user. Thus, the ideal profile needs to be determined for each spectrum individually.

A main advantage of the Gaussian distribution compared to other curve shapes (e.g., exponentially modified Gauss) for our application is that only two parameters, the width (σ) and the area (A) of the peak need to be determined (Formula 1):

$$f(t) = \frac{A}{\sigma\sqrt{2\pi}} e^{\frac{-1}{2}(\frac{t-t_x}{\sigma})^2}$$

Equation 1

This accelerates the algorithm, makes the score attribution more robust, and simplifies the interpretation of results. Thus, considering two mass peaks in the analysis, only four parameters need to be found for each single measurement. A least-square algorithm that minimizes the difference between the fitted curve and the measured data was implemented in MATLAB to obtain these parameters. The fitted curves for ^{56}Fe and ^{58}Ni are represented in red in the figures. If the distortion is so strong that no Gaussian can be fitted, a negative value is assigned to σ, leading to a negative score (Equation 3).

The difference between the ideal peak profile and the measured data gives a direct measure for the quality of the spectrum and minimal values could be used to select the best spectra. However, fluctuations in the intensities of the spectrum from one single measurement to another make it impossible to directly use the difference. Normalizing the error to the signal strength in the interval between the two mass peaks can provide a more reliable measure of the quality of the spectrum. This relative area error is defined as:

$$\Delta_A = \frac{\sum_{t2}^{t1} |m(t) - g(t)|}{\sum_{t2}^{t1} m(t)}$$

Equation 2

Where $m(t)$ is the discrete measured signal value at sample t (black line in Figure 2) and $g(t)$ is the fitted profile (red line), $t1$ is the midpoint of the first fitted peak and $t2$ the midpoint of the second fitted peak. The absolute error is taken to avoid that random fluctuations around the ideal profile compensate each other.

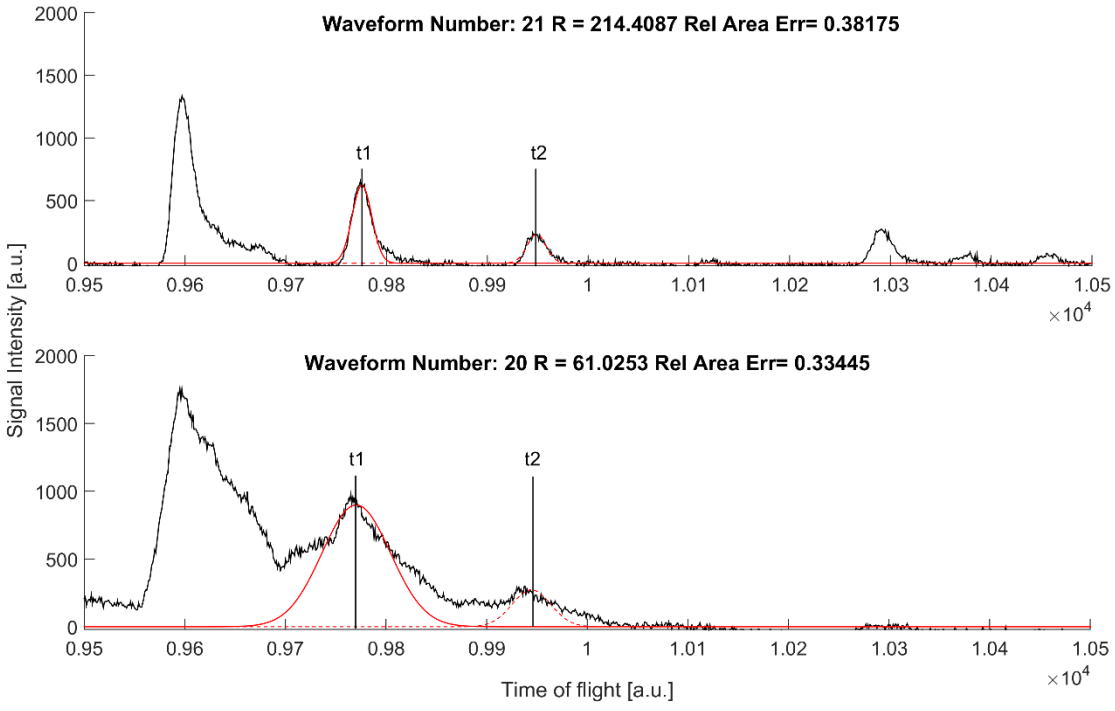

Figure 2: Similar relative area error for good and bad mass spectrum quality.

Figure 2 illustrates why the relative area error alone is not sufficient to assess the quality of the spectrum. The peak fit algorithm can approximate broad peaks with broad, high σ-Gaussian distribution curves, thereby minimising the relative area error for measurements of bad quality, which should be discarded. To cope with this effect, the mass resolution of the first fitted peak (Equation 1), is also taken into account for the calculation of the score. This allows to reject bad peaks efficiently.

$$R_1 = \frac{m}{\Delta m} = \frac{1}{2}\frac{t_1}{\Delta t_1} \cong \frac{1}{2}\frac{t_1}{2.355\sigma_1}$$

Equation 3

Because the relative error should be minimized and the resolution should be maximized the score for a spectrum can be defined as:

$$S = \frac{R_1}{\Delta_A}$$

Equation 4

Exclusion of spectra with a low score increases therefore the quality of the spectrum. After attributing a score to all spectra, an adequate trade-off between rejection of spectra and keeping a good statistic is required. A reliable and reproducible method for the threshold determination is presented below and illustrated on behalf of measurements made with our miniature LIMS system.

Setup and Materials

The measurements are conducted with our miniature laser mass spectrometer (LMS) composed of a grid-less reflectron-type TOF mass spectrometer and a femtosecond laser ablation ion source and is described in full detail in our previous publications[3, 6, 13, 15, 17]. In this contribution we only give a short overview of the system. The compact instrument prototype (~160 mm long and ∅60 mm), shown in Figure 3 was built for in-situ analysis on planetary surfaces[9]. The instrument is located in a vacuum chamber operated at pressures in the 10^{-8} mbar range. The investigated sample is positioned a fraction of a mm from the instrument's aperture, where the laser ($\lambda = 775$ nm, $\tau \sim 190$ fs, repetition rate ≤1 kHz, intensity ≤1 mJ/pulse) is focussed to a spot of 10–15 μm. Positively charged ions that are produced during the laser ablation/ionisation are accelerated and confined into the field free drift space through a series of electrodes. Subsequently, the beam is reflected and time-focussed on the detector by an ion mirror. The detector consists of two multi-channel plates (MCP) in chevron configuration mounted on a micro-strip five ring anode plate with four output signal channels[17]. This architecture allows measurements with dynamic ranges of up to 10^8 and sensitivities below ppm levels.

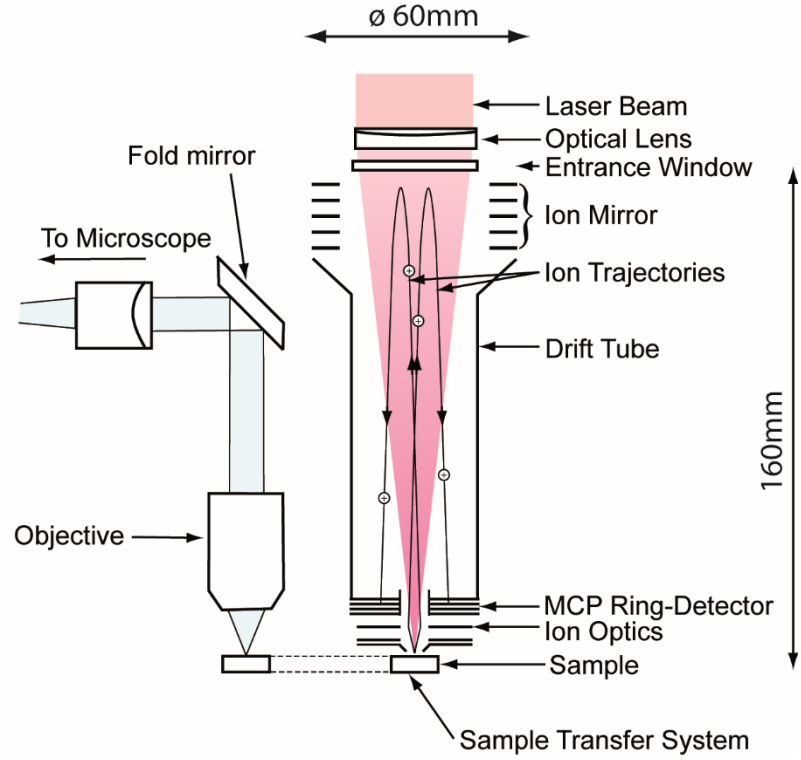

Figure 3: Schematic drawing of the LMS Instrument including LIMS TOF MS and Microscope System

Two 8 bit two channel ADC cards with a sampling speed of 4 GS/s are used to acquire the spectra. A custom-made microscope next to the mass spectrometer allows to locate features of interest in heterogeneous samples with μm precision[13]

For a homogeneous sample, large ion signal fluctuations are observed typically within the first laser shots when the ablation crater is being formed. The ablation of heterogeneous samples can produce more fluctuations in ion production during laser ablation. Heterogeneity is often encountered in minerals and other types of natural samples and potentially has an important influence on the crater formation and ablation process, sample conductivity as well as on the choice of the instrument settings required for optimal ablation. Thus, to demonstrate the performance of the method on a natural sample with known isotope composition, we analysed isotope ratios of key elements in the Trevorite mineral ($NiFe_2O_4$)[18] with spectra from an existing measurement campaign. During this campaign measurements were taken at 10 different locations at pulse energies of ~ 1 μJ/shot. On each location 230 up to 630 spectra were acquired, each one containing an accumulation of 100 laser cycles. Figure 1, panel c depicts a typical spectrum acquired on one location during this campaign.

Determination of threshold score

The first step after taking the measurement series is therefore to find an optimal threshold score that guarantees good statistics while removing the largest possible number of bad spectra. We found that a reliable and simple measure for determining the threshold score is to perform a parametric study on the peak/valley ratio between major peaks and their neighbouring valleys. The peak/valley ratio was calculated by dividing the peak signal intensity of the peak at m/q = X by the mean signal intensity in the interval from X+0.3 to X+0.8. For X the values 16, 25, 26, and 28 were chosen. The peak at m/q = 24 shows saturation effects and is therefore not suitable for determining the threshold value. Figure 4 shows the peak/valley ratios versus the threshold score. All curves have a maximum at a threshold score around 500. Below that value,

more distorted files are included in the accumulation process and the peak/valley ratio (i.e., spectral quality) decreases. Above the curve maximum, removing files from accumulation process has no effect on the quality of the spectrum but steadily decreases the SNR and thereby the peak/value ratio. Thus, the best choice for a threshold score is the maximum value at 500. It is remarkable that the maximum is surrounded by a broad plateau of ±200 where the choice of the threshold score does not have a significant influence on the peak/valley ratio, which means that a rough estimate of the maximum score is sufficient for obtaining good and robust results.

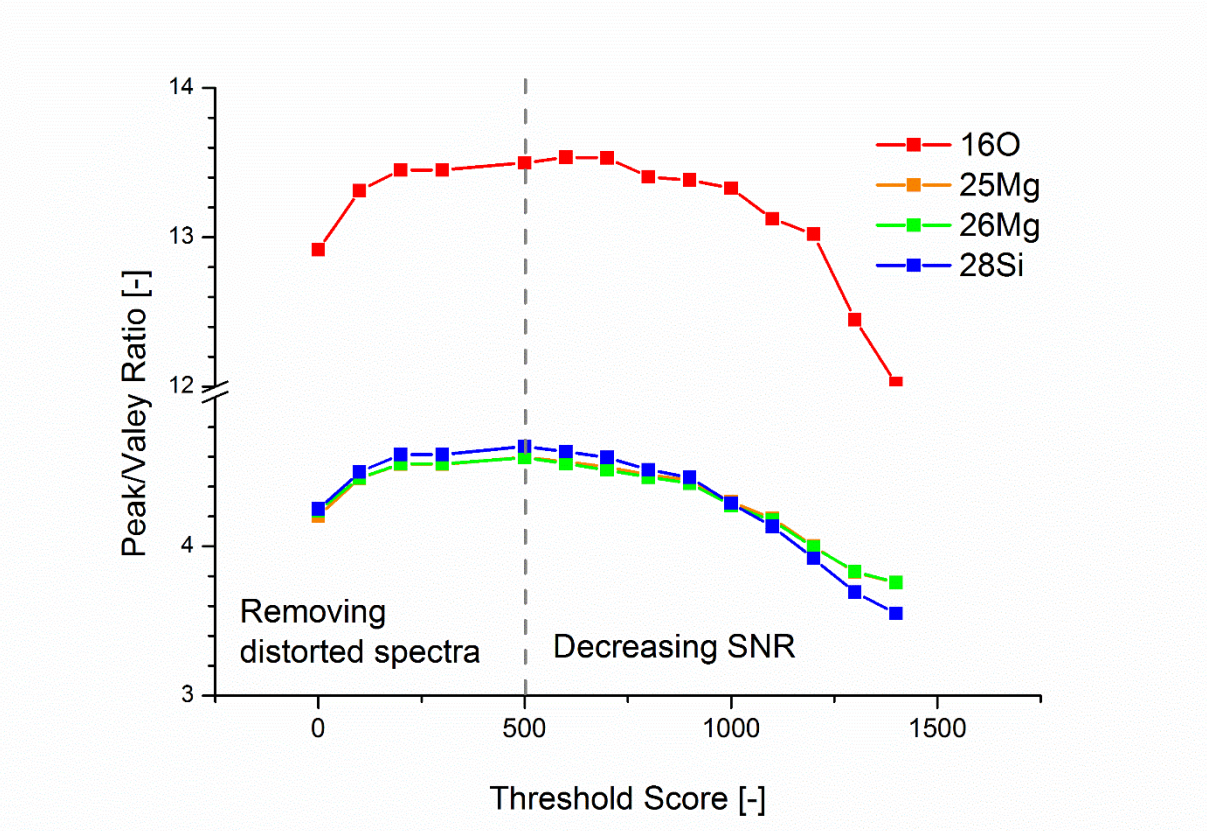

Figure 4: Determination of the threshold score (see text for explanation)

Once a threshold is determined for a data set (a measurement location on the sample), it should be applicable to any other location of a measurement campaign on the same sample, assuming that the same instrument settings were applied to acquire the spectra. We were able to prove this by evaluating the performance of the method on a series of 10 measurement locations, with the main interest to study the Ni isotope composition in the Trevorite. We focussed on the determination of the isotope ratios of the two main isotopes 58 and 60, since the SNR for the other isotopes 61, 62 and 63 was too low (< 10–15 for the ^{62}Ni unfiltered spectra series) for a thorough analysis. Moreover, the isotope 64 is also subjected to isobaric interference with traces of Zn or oxides (Mg_2O), see Figure 3.

Because the main element Mg suffers from saturation effects, we investigated the Si isotopes to study the performance of the method on major elements and the ^{52}Cr/^{53}Cr ratio as an additional minor element. Due to the presence of Mg_2 and Fe, it was not possible to analyse the other Cr peaks with sufficient accuracy. An approach to overcome the problem of isobaric interference with clusters and molecules is presented in one of our recent publications [19].

Moreover, the presence of Fe in the sample causes also a weak isobaric interference between the ^{58}Fe and ^{58}Ni isotopes. Assuming terrestrial isotope ratios[18, 20] the abundance of ^{58}Fe can be estimated as:

$$A_{Fe}^{58} \sim 0.00282/0.99718 * (A_{Fe}^{54} + A_{Fe}^{56} + A_{Fe}^{57}),$$

Equation 5

Therefore, the corrected abundance of ^{58}Ni is approximately:

$$A_{Ni}^{58} \approx A_{measured}^{58} - A_{Fe}^{58}$$

Equation 6

Results

The relative isotope accuracy is defined as:

$$IA_R = \frac{C_{meas} - C_{ref}}{C_{ref}}$$

Equation 7

where C_{meas} is the measured isotope ratio and C_{ref} is the isotope ratio in the standard[21-22]. The measured abundance is determined using peak area integration.[23]

The improvements to the derived relative isotope accuracy achieved by applying our spectrum filtering algorithm become visible when analysing mass spectra affected by effects of spectral degradation. Figure 5, lower panel, shows the histogram of all calculated scores on one location on the sample obtained by analysing the ^{58}Ni and ^{60}Ni peak. For 200 of the 238 spectra, the peak fitting was successful, resulting in a positive score. In 38 cases, the peak fit failed and a negative score was attributed to these files. Figure 5, lower panel, shows that at a threshold score of 500 is a suitable choice in terms of statistics because only a minor part of the spectra will be removed. Figure 5, upper panel, shows a typical distribution of the discarded files in the sequence of individual measurements. Many degraded spectra were recorded close to the surface (left side in Figure 5, upper panel). The initial crater formation process, to which we attribute many spectra of bad quality, occurs typically during the first 5'000 to 10'000 laser shots[24]. Afterwards, the mass peak intensities and mass resolution stabilize and only a few files have to be discarded in a random occurrence pattern. This threshold score guarantees a good averaging over the remaining measurement range once the crater is established.

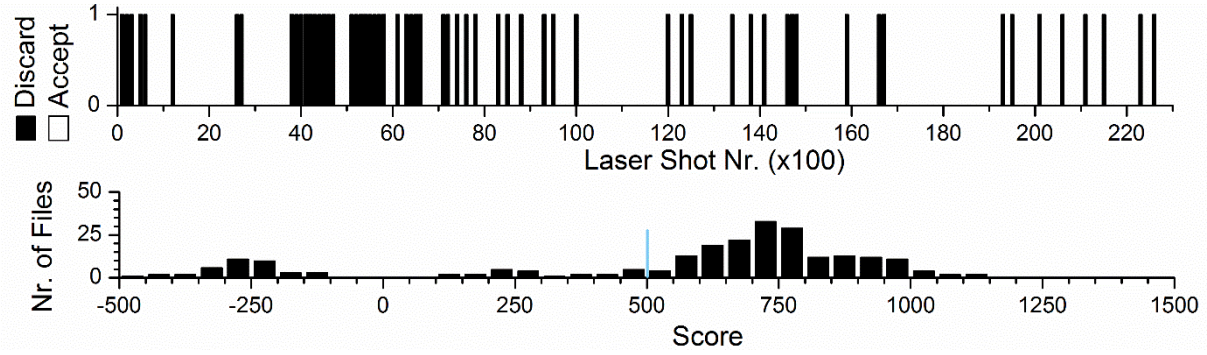

Figure 5: Accepted and discarded spectrum versus laser shot number (top panel); Histogram of scores for 238 spectra (lower panel). The blue line indicates the threshold value determined above.

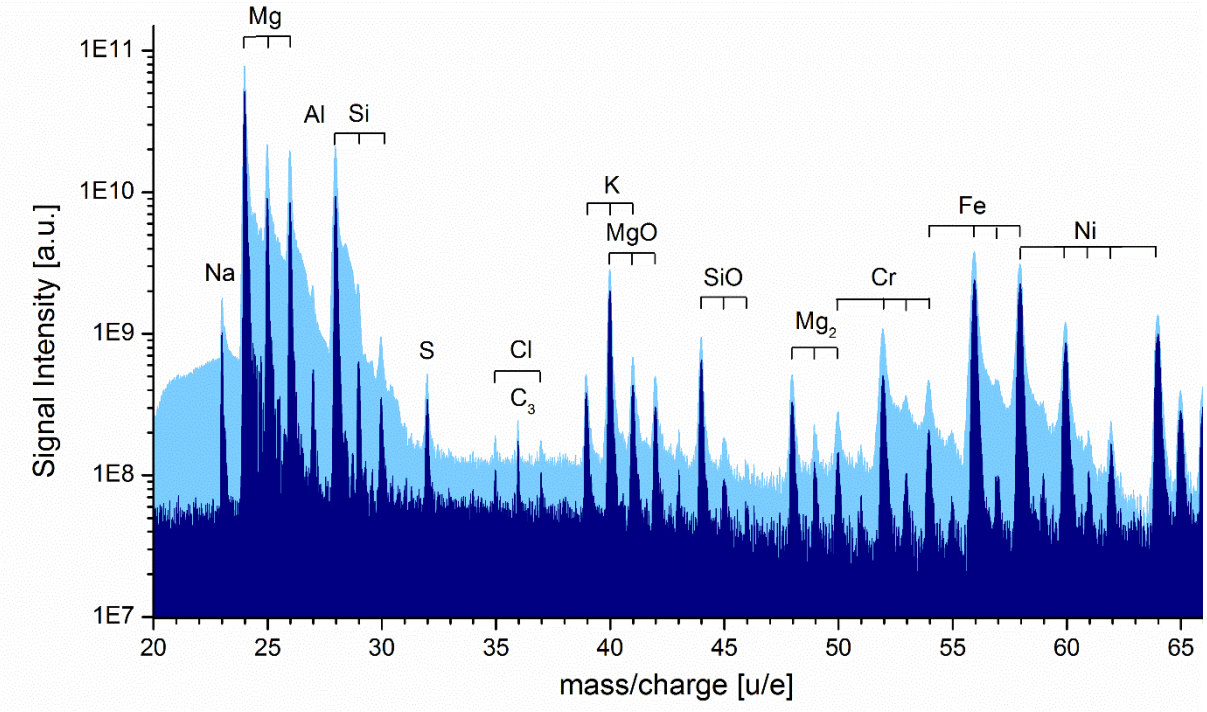

Figure 6: original (238 spectra, light blue) and filtered accumulation (dark blue), no further (noise) filtering was applied

After removing spectra with a score lower than the threshold score and subsequent accumulation, the spectrum displayed in dark blue on Figure 6 is obtained. To facilitate a direct comparison, the original unfiltered spectrum is also shown in light blue. After filtering, the peaks are much more distinct. Some mass peaks that were difficult to recognise in the original spectrum such as ^{27}Al are now readily distinguishable from the neighbouring Si and Mg peaks. The same is true for the Cr and Fe isotopes that are sufficiently resolved to conduct the quantitative isotope analysis.

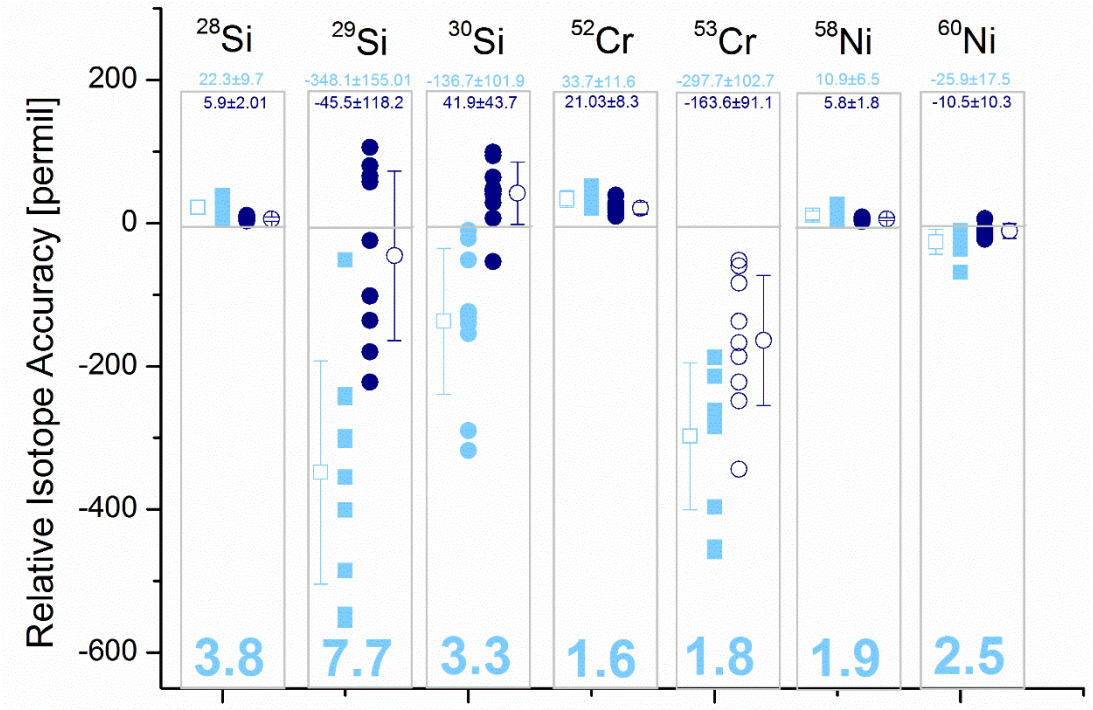

Figure 7: Relative Isotope accuracies for the unfiltered spectrum (light blue) and the filtered spectrum (dark blue). Open and closed symbols give the individual measurements and the mean of the measurements, respectively. The numbers at the top

of the boxes indicate the mean isotope accuracies and the standard deviation before and after the filtering process. The numbers at the bottom of the boxes correspond to the factor by which the isotope accuracy was improved.

A total of 70 isotope accuracies (7 isotope accuracies on 10 locations on the sample) were analysed using our in-house software[21] and the results are summarized in Figure 7. The light blue squares represent the relative isotope accuracy before and the dark blue circles represents the corresponding value after applying the filtering method. The outlined squares and circles indicate the mean relative isotope accuracy over all locations and the error bars show the standard deviation. The most important improvement was achieved on the ^{29}Si peak, where the relative isotope accuracy was improved by a factor of 7.7. For the other investigated relative isotope accuracies, an improvement factor in the range of 1.6–3.8 was achieved. All means of the measurements of the investigated isotopes improved due to the filtering, and for the individual measurements only 7 of the total 70 measured isotope ratios worsened after the filtering.

On three of the 10 locations, good results were achieved when only 26.9% – 57.5%, of the files were retained. On the remaining locations, only 8 to 30.8 % of the spectra were discarded and the losses of measurements are therefore in a more acceptable range.

Limitations

In some cases, the proposed filtering method does not recover a good quality spectrum or the method needs to be applied with caution. Using some examples encountered during our studies we present the limitations of the method in this section.

The method analyses and judges the shape of selected peaks regardless of their origin. The peaks under investigation could come from a specific isotope or any isobaric interference of several isotopes or clusters. If an isotope ratio is altered by a strong interference between elements and clusters, it is therefore unable to improve isotope ratios in such a case.

1. If signal ringing is present in the acquired spectrum, the method presented in this contribution cannot recover spectral quality. Because this type of distortion is in phase in all the files, eliminating a part of the files does not reduce the relative amplitude of the distortion and our method would not improve the result.

2. Sampling over the interface between two materials with strongly different ablation/ionisation efficiencies, can mislead the filtering algorithm. Spectra taken when sampling across the boundary will be changing because of changing material composition, changing ablation parameters, and possible matrix effects. Thus, the algorithm can potentially fail to fit peaks if it is present only in one of the two materials. This would then lead to partial or complete removal of one of the materials from the spectrum. This risk can be mitigated by analysing the information displayed in Figure 6 and comparing the unfiltered spectrum to the filtered spectrum. Using depth profiling information, as presented in previous publications[25-26] erroneous filtering and altering of spectra due to material transitions can be excluded with good confidence.

Conclusion

In this contribution we showed that distorted mass spectra can severely worsen the quality of the accumulated mass spectra, even if only a small fraction of the accumulated spectra are actually concerned. Using the simple and reproducible filtering process presented in this contribution, we were able to reliably remove the distorted spectra from the accumulation and improve both, mass resolution and relative isotope accuracy. After the filtering process, clearly

distinct peaks can be identified in previously unresolved portions of the mass spectrum. The isotope accuracies derived from the filtered spectrum were improved by factors of 1.6–7.7 for the investigated cases. We discussed limitations process and show examples where it has to be applied with caution.

Acknowledgments
We gratefully acknowledge the financial support of the Swiss National Science Foundation. H. Shea, Microsystems for Space Technologies Laboratory, Ecole Polytechnique Férérale Lausanne, Switzerland for his support.

References

1. Riedo, A.; Grimaudo, V.; Moreno-Garcia, P.; Neuland, M. B.; Tulej, M.; Broekmann, P.; Wurz, P., Laser Ablation/Ionisation Mass Spectrometry: Sensitive and Quantitative Chemical Depth Profiling of Solid Materials. *Chimia* **2016,** *70* (4), 268-273.
2. Zhang, B. C.; He, M. H.; Hang, W.; Huang, B. L., Minimizing Matrix Effect by Femtosecond Laser Ablation and Ionization in Elemental Determination. *Analytical Chemistry* **2013,** *85* (9), 4507-4511.
3. Riedo, A.; Bieler, A.; Neuland, M.; Tulej, M.; Wurz, P., Performance evaluation of a miniature laser ablation time-of-flight mass spectrometer designed for in situ investigations in planetary space research. *J Mass Spectrom* **2013,** *48* (1), 1-15.
4. Zhang, S. D.; He, M. H.; Yin, Z. B.; Zhu, E. Y.; Hang, W.; Huang, B. L., Elemental fractionation and matrix effects in laser sampling based spectrometry. *J Anal Atom Spectrom* **2016,** *31* (2), 358-382.
5. Huang, R. F.; Yu, Q.; Li, L. F.; Lin, Y. M.; Hang, W.; He, J.; Huang, B. L., High Irradiance Laser Ionization Orthogonal Time-of-Flight Mass Spectrometry: A Versatile Tool for Solid Analysis. *Mass Spectrom Rev* **2011,** *30* (6), 1256-1268.
6. Riedo, A.; Neuland, M.; Meyer, S.; Tulej, M.; Wurz, P., Coupling of LMS with a fs-laser ablation ion source: elemental and isotope composition measurements. *J Anal Atom Spectrom* **2013,** *28* (8), 1256-1269.
7. Neuland, M. B.; Grimaudo, V.; Mezger, K.; Moreno-Garcia, P.; Riedo, A.; Tulej, M.; Wurz, P., Quantitative measurement of the chemical composition of geological standards with a miniature laser ablation/ionization mass spectrometer designed for in situ application in space research. *Meas Sci Technol* **2016,** *27* (3).
8. Riedo, A.; Meyer, S.; Heredia, B.; Neuland, M. B.; Bieler, A.; Tulej, M.; Leya, I.; Iakovleva, M.; Mezger, K.; Wurz, P., Highly accurate isotope composition measurements by a miniature laser ablation mass spectrometer designed for in situ investigations on planetary surfaces. *Planet Space Sci* **2013,** *87*, 1-13.
9. Rohner, U.; Whitby, J. A.; Wurz, P., A miniature laser ablation time-of-flight mass spectrometer for in situ planetary exploration. *Meas Sci Technol* **2003,** *14* (12), 2159-2164.
10. Managadze, G. G.; Wurz, P.; Sagdeev, R. Z.; Chumikov, A. E.; Tuley, M.; Yakovleva, M.; Managadze, N. G.; Bondarenko, A. L., Study of the main geochemical characteristics of Phobos' regolith using laser time-of-flight mass spectrometry. *Solar Syst Res+* **2010,** *44* (5), 376-384.
11. Li, X.; Brinckerhoff, W. B.; Managadze, G. G.; Pugel, D. E.; Corrigan, C. M.; Doty, J. H., Laser ablation mass spectrometer (LAMS) as a standoff analyzer in space missions for airless bodies. *Int J Mass Spectrom* **2012,** *323*, 63-67.
12. Tulej, M.; Iakovleva, M.; Leya, I.; Wurz, P., A miniature mass analyser for in-situ elemental analysis of planetary material-performance studies. *Analytical and Bioanalytical Chemistry* **2011,** *399* (6), 2185-2200.
13. Wiesendanger, R.; Wacey, D.; Tulej, M.; Neubeck, A.; Ivarsson, M.; Grimaudo, V.; Moreno-Garcia, P.; Cedeño López, A.; Riedo, A.; Wurz, P., Chemical and optical identification of micrometre

sized 1.9 billion-year-old fossils with a miniature LIMS system combined with an optical microscope. *Astrobiology* **2018,** *[subm.]*.
14. Tulej, M.; Neubeck, A.; Ivarsson, M.; Riedo, A.; Neuland, M. B.; Meyer, S.; Wurz, P., Chemical Composition of Micrometer-Sized Filaments in an Aragonite Host by a Miniature Laser Ablation/Ionization Mass Spectrometer. *Astrobiology* **2015,** *15* (8), 669-82.
15. Wiesendanger, R.; Tulej, M.; Riedo, A.; Frey, S.; Shea, H.; Wurz, P., Improved detection sensitivity for heavy trace elements using a miniature laser ablation ionisation mass spectrometer. *J Anal Atom Spectrom* **2017**.
16. Brinckerhoff, W. B.; Managadze, G. G.; McEntire, R. W.; Cheng, A. F.; Green, W. J., Laser time-of-flight mass spectrometry for space. *Rev Sci Instrum* **2000,** *71* (2), 536-545.
17. Riedo, A.; Tulej, M.; Rohner, U.; Wurz, P., High-speed microstrip multi-anode Multichannel Plate Detector System. *Rev. Sci. Instrum* **2017,** *[subm.]*.
18. Gueguen, B.; Rouxel, O.; Ponzevera, E.; Bekker, A.; Fouquet, Y., Nickel Isotope Variations in Terrestrial Silicate Rocks and Geological Reference Materials Measured by MC-ICP-MS. *Geostand Geoanal Res* **2013,** *37* (3), 297-317.
19. Tulej, M.; Wiesendanger, R.; Riedo, A.; Knopp, G.; Wurz, P., Mass spectrometric analysis of Mg-plasma produced by a double-pulse femtosecond laser irradiation. *J Anal Atom Spectrom* **2018,** *[subm.]*.
20. Becker, J. S., *Inorganic mass spectrometry principles and applications*. John Wiley: Chichester, 2007; p Online-Ressource.
21. Meyer, S.; Riedo, A.; Neuland, M. B.; Tulej, M.; Wurz, P., Fully automatic and precise data analysis developed for time-of-flight mass spectrometry. *J. Mass Spectrom* **2017,** *[subm.]*.
22. Becker, J. S., *Inorganic Mass Spectrometry*. John Wiley & Sons Ltd.: 2007.
23. Meyer, S.; Riedo, A.; Neuland, M. B.; Tulej, M.; Wurz, P., Fully automatic and precise data analysis developed for time-of-flight mass spectrometry. *Journal of Mass Spectrometry* **2017,** *52* (9), 580-590.
24. Grimaudo, V.; Moreno-Garcia, P.; Lopez, A. C.; Riedo, A.; Wiesendanger, R.; Tulej, M.; Gruber, C.; Lortscher, E.; Wurz, P.; Broekmann, P., Combining Anisotropic Etching and PDMS Casting for Three-Dimensional Analysis of Laser Ablation Processes. *Analytical Chemistry* **2018,** *90* (4), 2692-2700.
25. Grimaudo, V.; Moreno-Garcia, P.; Riedo, A.; Meyer, S.; Tulej, M.; Neuland, M. B.; Mohos, M.; Gutz, C.; Waldvogek, S. R.; Wurz, P.; Broekmann, P., Toward Three-Dimensional Chemical Imaging of Ternary Cu-Sn-Pb Alloys Using Femtosecond Laser Ablation/Ionization Mass Spectrometry. *Analytical Chemistry* **2017,** *89* (3), 1632-1641.
26. Grimaudo, V.; Moreno-Garcia, P.; Riedo, A.; Neuland, M. B.; Tulej, M.; Broekmann, P.; Wurz, P., High-resolution chemical depth profiling of solid material using a miniature laser ablation/ionization mass spectrometer. *Anal Chem* **2015,** *87* (4), 2037-41.